Hindawi
International Journal of RF and Microwave Computer-Aided Engineering
Volume 2023, Article ID 9669195, 7 pages
https://doi.org/10.1155/2023/9669195

Research Article

Broadband RCS Reduction Using Circular Sector Structure

Huijuan Dai,[1] **Po Li**,[1] **ShuYing Li**,[2] **WenJun Qi**,[2] **Chen Yu**,[2] **and YanQin Ma**[1]

[1]*Nanjing Vocational University of Industry Technology, Nanjing, China*
[2]*College of Electronic and Information Engineering, Nanjing University of Aeronautics and Astronautics, Nanjing, China*

Correspondence should be addressed to Huijuan Dai; daihuijuan519@163.com

Received 13 October 2022; Revised 28 December 2022; Accepted 1 March 2023; Published 29 June 2023

Academic Editor: He-Xiu Xu

In this paper, a new metasurface structure is designed to reduce radar cross section (RCS). In order to reduce the radar cross section (RCS), a new metasurface structure is designed. The unit adopts the polarization conversion metasurface structure, which is composed of asymmetric double arrow-shaped metal structure and etched on the dielectric substrate on the back of the metal plate. This polarization conversion metasurface (PCM) unit consists of asymmetric double arrow-shaped metal structure, and it is etched on a dielectric substrate backed with metallic plate. It can realize converting linear polarized waves to orthogonal ones in a broadband from 18.1 GHz to 32.7 GHz efficiently. According to the further development of the triangle chessboard layout, we also designed several new circular fan-shaped configurations, which realize RCS reduction in a wider -10 dB bandwidth compared with the triangle chessboard configuration. Finally, an optimized 8-lobed circular sector configuration composed of the designed PCM unit is selected for processing and testing. It can realize the RCS reduction greater than 10 dB in a wide bandwidth ranging from 13.7 GHz to 27.5 GHz, compared with the equal-sized metallic-backed dielectric substrate plate. The experimental results basically agree with the simulation ones. The proposed broadband circular sector structure has broad application prospects such as phased array antenna technology, electromagnetic stealth technology, and electromagnetic absorption technology.

1. Introduction

RCS reduction has important applications in many fields, especially in military stealth and antenna design. In recent years, the research on RCS reduction which is based on metasurface has aroused extensive interest of scholars [1–4]. Several RCS reduction technologies have been developed, such as electromagnetic band gap and high impedance surface; due to their narrow bandwidth, their applications are limited [5–7]. In recent years, more and more scholars turn to AMC (artificial magnetic conductor) structure to achieve broadband RCS reduction. The principle is based on the cancellation interference between AMC and PEC (perfect electric conductor) units which form the chessboard structure [6]. In order to further broaden the bandwidth of monostatic RCS reduction greater than 10 dB, a variety of means have been tried. Among them, one effective mean is to replace the original combination of AMC and PEC units by using one AMC unit with different sizes to form the chessboard structure [8–10]. Through the above methods, the RCS reduction bandwidth of target can be greatly improved, but this is at the cost of structural complexity.

Moreover, polarization-dependent AMC has been designed by using one AMC unit to simplify the design procedure [11, 12]. The selected AMC unit is a PCM structure with an ultra-wideband and a high polarization conversion rate (PCR). The 180° phase difference can be satisfied between a PCM unit and its mirror one in the orthogonal direction, which guarantees the broadband RCS reduction bandwidth. The circular structure which is composed of PCM unit to realize RCS reduction has the advantages of a simpler structure, a wider bandwidth, and easier combination with antennas.

In order to obtain a wider bandwidth of RCS reduction, the designed unit must have a high PCR in a wideband. In this paper, a new ultra-wideband polarization conversion structure is proposed. The relative bandwidth of the PCR above 90% is 90.3%. Then, the PCM unit is arranged in

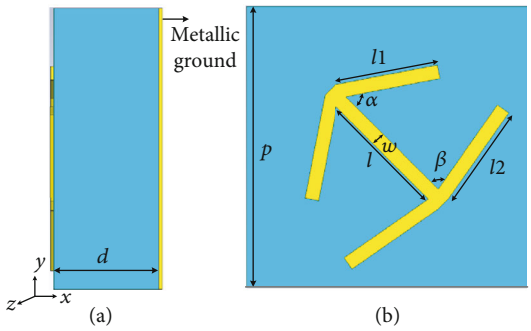

FIGURE 1: (a) Side view and (b) front view of the unit.

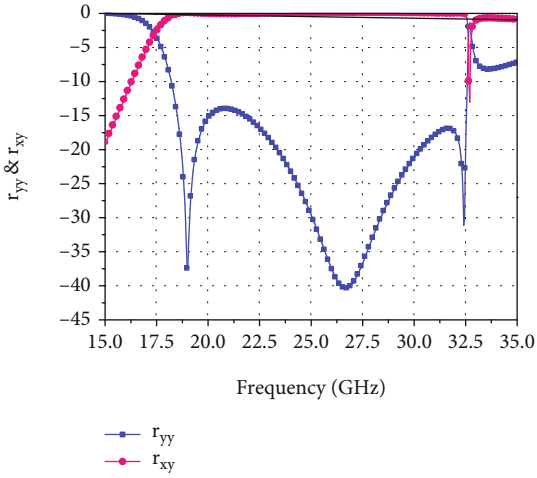

FIGURE 2: Reflection coefficient r_{xy} and r_{yy} of the PCM unit.

two different chessboard structures, and the simulation results show that RCS reduction in a wider band can be realized in the triangle chessboard structure than the square one.

2. Design of the Unit

2.1. Structure and Principle of Unit. The principle of chessboard structure is based on the interference cancellation of two different AMC structures that constitute the chessboard. By rotating the same PCM unit 90°, the phase difference between the two mirror symmetrical structures is always maintained at 180°.

Figure 1 shows a diagram of the designed PCM unit. The specific geometric parameters of the unit are given as periodic side length of unit $p = 4$ mm, length of the middle stub $l = 2.3$ mm, line width $w = 0.2$ mm, arrow line length l_1 and l_2 both 1.5 mm, thickness of the dielectric substrate $d = 1.5$ mm, and included angle $\alpha = 56°$ and $\beta = 80°$. The asymmetric double arrow-shaped structure and the metallic plate on the back surface are all made of copper. And F4B (dielectric constant $\varepsilon_r = 2.2$ and loss tangent $\tan\delta = 0.001$) is selected as the dielectric substrate. This PCM structure can expand the polarization conversion bandwidth by exciting multiple resonant modes [13].

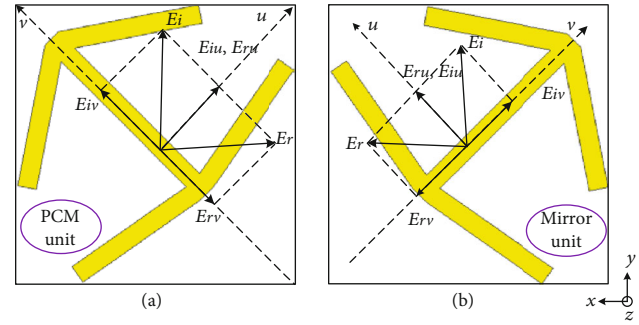

FIGURE 3: Schematic diagram of x-to-y polarization conversion: (a) PCM unit and (b) its mirror one.

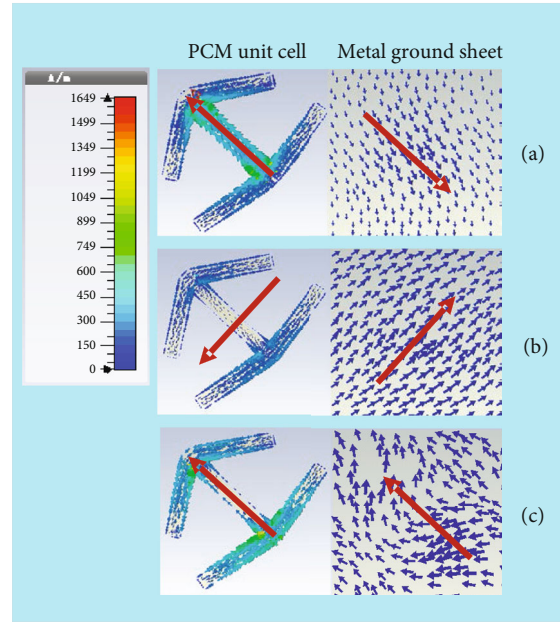

FIGURE 4: The surface current distribution of this PCM structure on the upper surface of the PCM unit and the metal grounding plate on the lower surface at the three resonant frequencies: (a) 19 GHz, (b) 26.7 GHz, and (c) 32.4 GHz.

CST Microwave Studio is used to optimize the structure. The reflection coefficients r_{xy} and r_{yy} are shown in Figure 2. Here, r_{xy} and r_{yy} are defined to represent the cross-polarization reflection coefficient and copolarization reflection coefficient, respectively [13]. We can see that the PCR between 18.1 GHz and 32.7 GHz can reach more than 90% under a normally incident wave. Taking an incident wave polarized in the y-axis as an example, the PCR is defined as

$$\mathrm{PCR} = \frac{r_{xy}^2}{r_{xy}^2 + r_{yy}^2} = \frac{r_{yx}^2}{r_{yx}^2 + r_{xx}^2}. \quad (1)$$

The values of r_{xy} and r_{yy} versus frequency are presented in Figure 2. The -10 dB polarization conversion bandwidth of the unit is from 18.1 GHz to 32.7 GHz, as shown in Figure 2. The average PCR is almost 100% within the bandwidth.

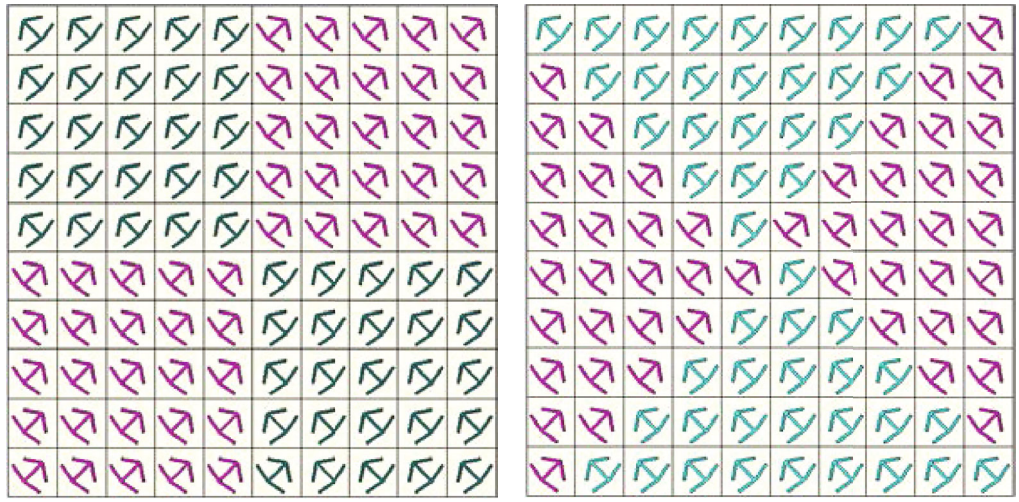

(a) (b)

Figure 5: Schematic diagram of PCM unit arrangement in (a) square chessboard structure and (b) the triangle chessboard one.

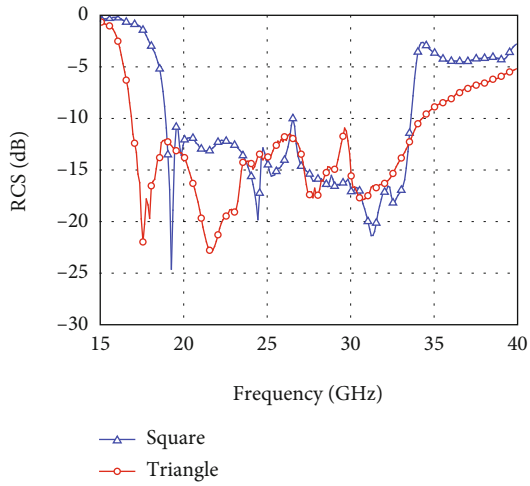

Figure 6: Comparison diagram of RCS reduction.

2.2. Mechanism of Broadband PCM. To analyze the principle of polarization rotation characteristic of an asymmetric double arrow-shaped structure, the schematic diagram is shown in Figure 3. The "symmetrical" and "antisymmetrical" modes can be generated by the electric field components along the u- and v-axes, respectively.

In order to understand the polarization conversion principle of PCM, we assume that the incident wave is linearly polarized along the y-axis. The electric field can be decomposed into two mutually perpendicular components in the u and v directions, as shown in Figure 3. Therefore, the electric field of the incident electromagnetic wave can be expressed as

$$E = \tilde{r}_u u E_{iu} e^{j\varphi} + \tilde{r}_v v E_{iv} e^{j\varphi}, \quad (2)$$

and the electric field of the reflected wave can be written as

$$E_r = \tilde{r}_u u E_{iu} e^{j\phi} + \tilde{r}_v v E_{iv} e^{j\phi}. \quad (3)$$

r_u and r_y, respectively, represent the reflection coefficients of the u-axis and v-axis [14, 15]. Due to the anisotropy of the PCM unit structure, a phase difference $\Delta\varphi$ between $\tilde{r}_u$ and $\tilde{r}_v$ can be produced. As shown in Figure 3(b), the synthetic field for E_{ru} and E_{ry} will be along the x-axis, and the incident wave is rotated by 90° when $\Delta\boldsymbol{\varphi} \approx \pi$, and their modulus satisfies $r_u \approx r_v$. Here, we use the numbers "0" and "1" to represent the basic unit in Figure 3(a) and its mirror one in Figure 3(b).

To further study the physical mechanism of ultrawideband PCM, we observe the surface current distribution of the artificial electromagnetic structure on the upper surface of the PCM unit and the metal grounding plate on the lower surface at 19 GHz, 26.7 GHz, and 32.4 GHz, respectively. The large red arrows in Figures 4(a)–4(c) indicate the main current direction, respectively. It is seen clearly from Figures 4(a)–4(c) that the resonances formed by the upper and lower surface currents at 19 GHz and 26.7 GHz are magnetic resonances, while the resonance at 32.4 GHz is electric resonance. The adjacent multiresonance characteristic can increase the bandwidth of polarization conversion.

2.3. The Proposed PCM Chessboard Structure. Using the designed PCM unit, square and triangle chessboards are arranged, respectively, as shown in Figure 5. The chessboard structure contains 10×10 units. It is compared with the same size metal backing dielectric substrate.

In order to study the scattering field patterns of the two chessboards in Figures 5(a) and 5(b), the monostatic RCS reduction and scattered field are shown in Figures 6 and 7, respectively. It can be seen from Figure 6 that the -10 dB monostatic RCS reduction bandwidth of the square and triangle chessboards ranges from 19.0 GHz to 26.6 GHz and 16.9 GHz to 34.4 GHz, respectively.

Figure 7 intuitively presents the 3-D monostatic scattering of the equal-sized metallic-backed dielectric substrate

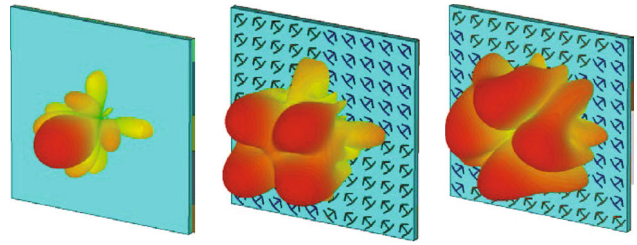

(a) (b) (c)

Figure 7: 3-D monostatic scattered fields at 17 GHz for (a) equal-sized metallic plate, (b) square chessboard, and (c) triangle one.

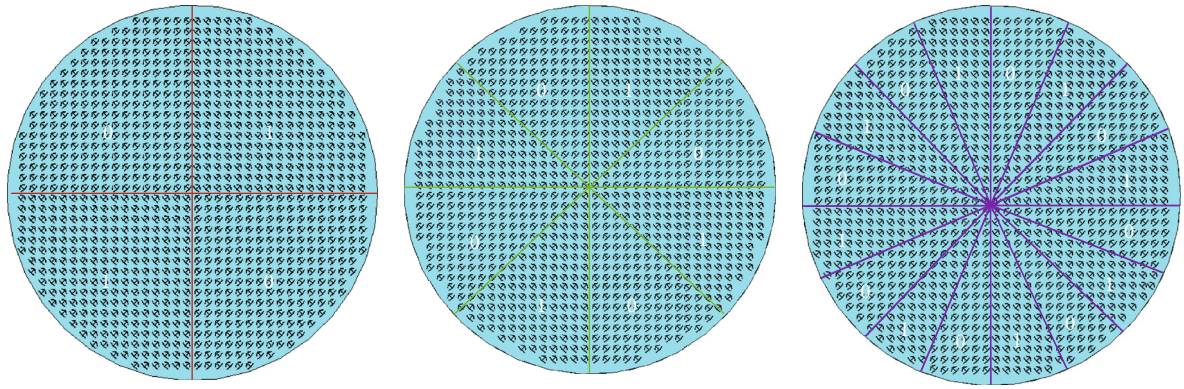

(a) (b) (c)

Figure 8: Three kinds of arrangement are as follows: (a) 4-lobe, (b) 8-lobe, and (c) 16-lobe circular fan-shaped structure.

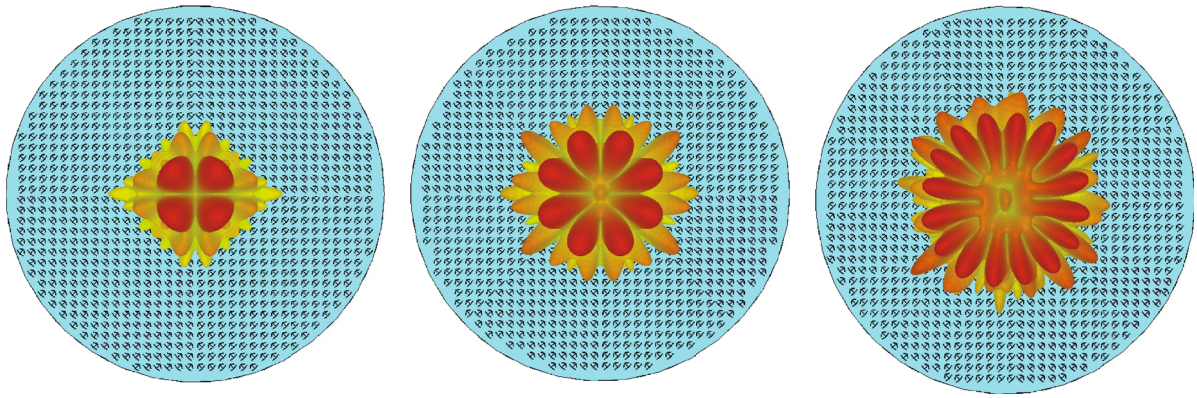

(a) (b) (c)

Figure 9: 3-D monostatic scattered fields at (a) 14.5 GHz, (b) 14.5 GHz, and (c) 17.5 GHz.

plate, square chessboard, and triangle chessboard at 17 GHz, respectively. The RCS of square and triangle PCM chessboard structures decreases greatly in the normal direction, due to the presence of four reflected lobes. In other words, the RCS reduction near the normal direction is on the energy reorientation in the nonvertical direction, and the backscattering effect of a triangle chessboard is better.

In addition, according to the further extension of the triangle chessboard arrangement, we also designed three circular fan-shaped chessboard arrangements, as shown in Figure 8. Compared with the triangle chessboard arrangement, the circular fan-shaped chessboard arrangement is called 4-lobe sector fan-shaped structure, 8-lobe sector fan-shaped structure, and 16-lobe sector fan-shaped structure, respectively, according to the number of backscattering lobes they produced.

The numbers "0" and "1", respectively, represent the asymmetric double arrow-shaped PCM units and their mirror ones. The "0" and "1" elements in Figure 8(a) divide the whole circle into four sectors; the "0" and "1" elements in Figure 8(b) divide the whole circle into eight sectors; and the "0" and "1" elements in Figure 8(c) divide the whole circle into 16 sectors.

When the incident electromagnetic wave is perpendicular to the surface of each circular fan-shaped arrangements, the backscattering patterns are shown in Figures 9(a)–9(c).

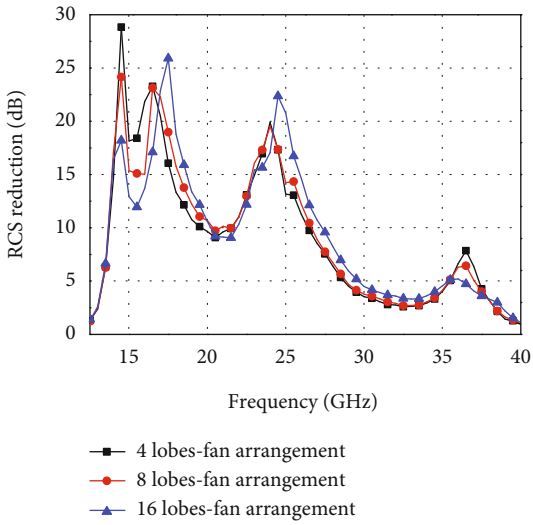

Figure 10: Schematic diagram of RCS reduction simulation results of 4-lobe, 8-lobe, and 16-lobe fan structures.

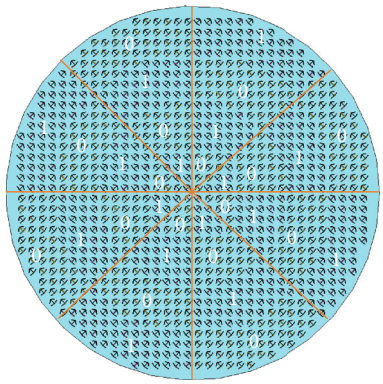

Figure 11: Photograph of the fabricated PCM circular fan-shaped arrangement.

It can be seen that the number and direction of backscattering lobes can be flexibly controlled by artificially changing the arrangement of these units and their mirror ones, and an effective reduction of backward RCS can be achieved. The RCS reduction effect is shown in Figure 10. It can be seen that with the increasing number of lobes, the -10 dB RCS reduction bandwidth also gradually widens.

As shown in Figure 11, for the optimized 8-lobed sector structure, the circular fan-shaped arrangement alternately arranges PCM units and their mirror ones with a phase difference of 180° along the radial direction, and the backscattering beams are scattered to the corresponding 8 directions, from inside to outside, and each four-layer element is alternately arranged in a fan-shaped outward divergent arrangement. Figure 12 shows the simulation diagram of the RCS reduction effect of the optimized 8-lobed sector structure.

We can see that the -10 dB RCS reduction bandwidth is from 13.7 GHz to 27.5 GHz, the relative bandwidth is 66.7%, and the maximum RCS reduction is 31.28 dB.

It can be seen from Figures 9(a)–9(c) that with more and more changes in the reflected phase arrangement of the metasurface, there are also more and more backscattering sidelobes,

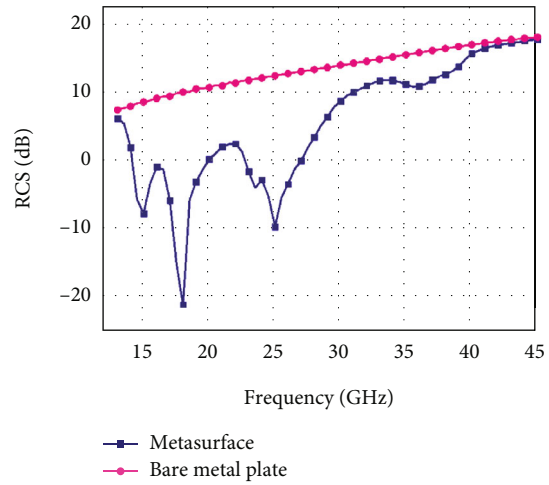

Figure 12: Simulated monostatic RCS reduction.

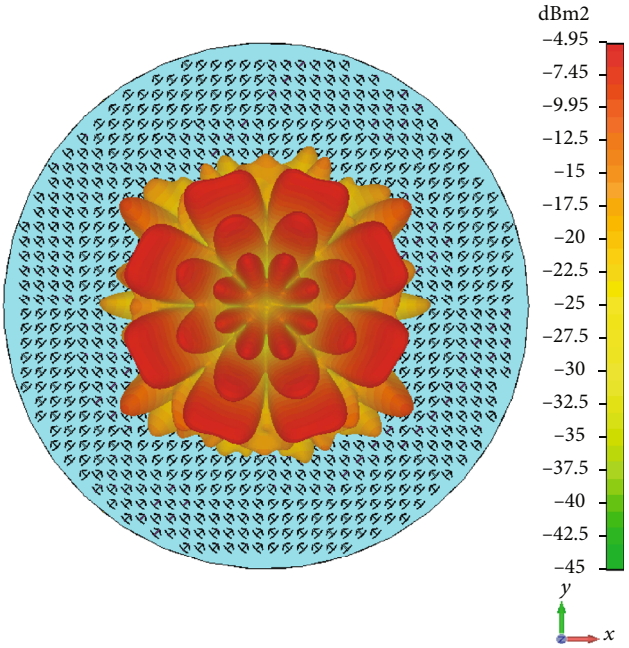

Figure 13: Simulation of far-field scattering pattern at 17.5 GHz.

and the energy of the main lobe is obviously reduced more and more, thus effectively reducing backscattering. If it is further extended to the coding metasurface, taking 1-bit coding metasurface as an example, as shown in Figure 11, the arrow 45° to the upper right corresponds to coding "1," and the arrow 45° to the upper left corresponds to coding "0." Figure 12 shows its corresponding far-field scattering. Figure 12 shows the corresponding far-field scattering diagram. It can be seen that the sidelobe is more scattered and the main lobe energy is reduced more obviously. Therefore, the backscattering effect is better. It is further speculated that if the coding sequence is further increased, more scattering directions will be obtained, which is more conducive to weakening the energy of the backscattering main lobe. At the same time, the scattering direction can be manually controlled to realize the intelligent material design.

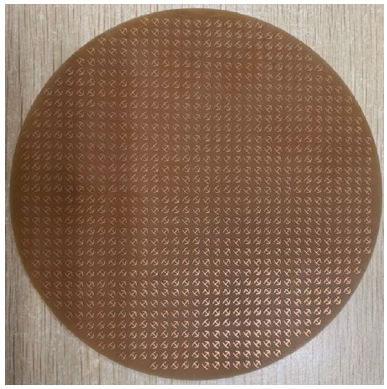

Figure 14: Schematic diagram of designed sample.

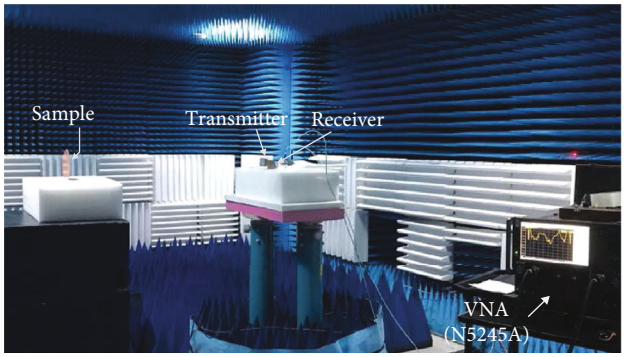

Figure 15: Experimental setup in the anechoic chamber.

Simulation of the far-field scattering pattern at 17.5 GHz shown is in Figure 13. It can be seen that the reflected waves are scattered in many directions like petals, which significantly reduces the size of the main lobe, thus effectively reducing the backscattering.

Therefore, the proposed structure combining chessboard structure with coding metasurface realizes the multidirectional scattering of electromagnetic wave. Compared with random coding structure, the proposed structure can more artificially control the regularity of electromagnetic wave scattering, while the electromagnetic wave direction of random scattering is disordered.

3. Fabrication and Measurement of the Proposed PCM Structure

To experimentally demonstrate that the proposed PCM structure can achieve wideband RCS reduction performance, the designed PCM is fabricated in an optimized triangle structure with an overall size of $\pi \times 722\,\text{mm}^2$ and contains 936 units, as shown in Figure 14. The experimental equipment and environment are shown in Figure 15. Two pairs of identical horn antennas are selected as transmitters and receivers covering the bandwidth from 12 GHz to 27 GHz, corresponding to the following two bands: 12 GHz-18 GHz and 18 GHz-26 GHz. The transmitting antenna and receiving antenna are, respectively, connected to both ends of the vector network analyzer. During the measurement, we need to keep the center of the sample, the transmitting antenna, and the receiving antenna at the same level.

Table 1: Comparison with other metasurface for RCS reduction.

	OB (GHz)	d (mm)	p (mm)
Ref. [16]	7.9-19.2	3	6
Ref. [17]	8.1-14.5	3.175	15
Present study	13.7-27.5	1.5	4

p: unit cell periodicity of the polarization converter; d: dielectric substrate thickness of the polarization converter; OB: operating bandwidth (PCR > 90%).

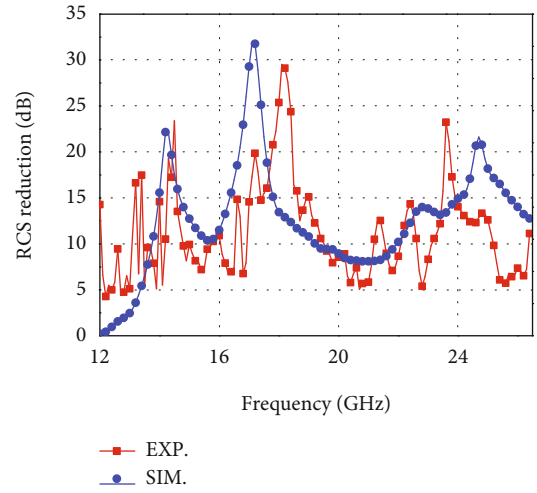

Figure 16: Comparison between simulation and measurement of monostatic RCS reduction effect.

The measurement results of RCS reduction are basically consistent with the simulation ones, but there are some errors and formant shifts, which may be caused by the following reasons: (1) the plane wave used in the experiment is generated by the far-field radiation of the horn antennas, while the ideal plane wave is used in simulation, and (2) fabrication tolerance and the error caused in the test, etc.

As shown in Table 1, the circular sector asymmetric structure proposed in this article has a working bandwidth (OB) of 13.7 GHz-27.5 GHz with a PCR greater than 90%, which is better than the working bandwidth of references [16, 17]. Moreover, it has a thinner thickness and a smaller cycle. Thus, the RCS reduction performance is relatively better.

The simulation and test results of the RCS reduction of the optimized 8-lobe sector structure under normal incidence are shown in Figure 16. The measurement results of RCS reduction are basically consistent with the simulation ones, but there are some errors and the shift of resonance peaks to some extent.

4. Conclusion

A novel 8-lobe sector PCM structure for broadband RCS reduction is designed in this paper. The upper surface of the PCM unit is an asymmetric double arrow-shaped resonator that has the ability of converting linear polarization wave into an orthogonal one. A 1-bit coding is combined

with sector structure to further improve the effect of backward RCS reduction. Because of the high PCR of the PCM unit, the designed new PCM circular sector structure can reduce RCS above 10 dB in an ultrawide bandwidth ranging from 13.7 GHz to 27.5 GHz, compared with the equal-sized metallic-backed dielectric substrate plate. To experimentally verify the designed structure, an optimized 8-lobed sector structure arranged by the designed PCM unit is fabricated and tested. The test results basically agree with the simulation ones.

Data Availability

The data used to support the findings of this study are included within the article.

Conflicts of Interest

The authors declare that they have no conflicts of interest.

Acknowledgments

The authors are grateful for the Research Initiation Fund of the Nanjing Vocational University of Industry Technology (YK22-02-02).

References

[1] S. Y. Li, L. L. Liu, Y. Y. Jiang, C. Z. Tang, C. Q. Gu, and Z. Li, "Ultrathin optically transparent electromagnetic shielding window with broadband microwave absorption and ultrahigh optical transmittance," *International Journal of RF and Microwave Computer-Aided Engineering*, vol. 32, no. 11, article e23338, 2022.

[2] S. Y. Li, L. L. Liu, Y. Y. Jiang, C. Z. Tang, C. Q. Gu, and Z. Li, "Ultrathin optically transparent metamaterial absorber for broadband microwave invisibility of solar panels," *Journal of Physics D: Applied Physics*, vol. 55, no. 4, article 045101, 2022.

[3] F. Costa, A. Monorchio, and G. Manara, "Analysis and design of ultra thin electromagnetic absorbers comprising resistively loaded high impedance surfaces," *IEEE Transactions on Antennas and Propagation*, vol. 58, no. 5, pp. 1551–1558, 2010.

[4] Y. Q. Li, H. Zhang, Y. Q. Fu, and N. C. Yuan, "RCS reduction of ridged waveguide slot antenna array using EBG radar absorbing material," *IEEE Antennas and Wireless Propagation Letters*, vol. 7, pp. 473–476, 2008.

[5] R. L. Fante and M. McCormack, "Reflection properties of the Salisbury screen," *IEEE Transactions on Antennas and Propagation*, vol. 36, no. 10, pp. 1443–1454, 1988.

[6] M. Paquay, J. C. Iriarte, I. Ederra, R. Gonzalo, and P. De Maagt, "Thin AMC structure for radar cross-section reduction," *IEEE Transactions on Antennas and Propagation*, vol. 55, no. 12, pp. 3630–3638, 2007.

[7] J. C. Iriarte Galarregui, A. Tellechea Pereda, J. L. M. De Falcon, and I. Ederra, "Broadband radar cross-section reduction using AMC technology," *IEEE Transactions on Antennas and Propagation*, vol. 61, no. 12, pp. 6136–6143, 2013.

[8] A. Edalati and K. Sarabandi, "Wideband, wide angle, polarization independent RCS reduction using nonabsorptive miniaturized-element frequency selective surfaces," *IEEE Transactions on Antennas and Propagation*, vol. 62, no. 2, pp. 747–754, 2014.

[9] W. Chen, C. Balanis, and C. R. Birtcher, "Checkerboard EBG surfaces for wideband radar cross section reduction," *IEEE Transactions on Antennas and Propagation*, vol. 63, no. 6, pp. 2636–2645, 2015.

[10] F. Yang and Y. Rahmat-Samii, "Polarization-dependent electromagnetic band gap (PDEBG) structures: designs and applications," *Microwave and Optical Technology Letters*, vol. 41, no. 6, pp. 439–444, 2004.

[11] Y. Zhao, C. Yu, J. Gao et al., "Broadband metamaterial surface for antenna RCS reduction and gain enhancement," *IEEE Transactions on Antennas and Propagation*, vol. 99, pp. 1–1, 2018.

[12] H. J. Dai, Y. J. Zhao, H. Y. Sun, J. Q. Chen, Y. Ge, and Z. Li, "An ultra-wideband linear polarization conversion metasurface," *Japanese Journal of Applied Physics*, vol. 57, no. 9, article 090311, 2018.

[13] H. J. Dai, Y. J. Zhao, J. Q. Chen, C. Yu, and L. Xing, "Ultra-wideband radar cross-section reduction using polarization conversion metasurface," *International Journal of RF and Microwave Computer-Aided Engineering*, vol. 30, no. 2, p. 22085, 2020.

[14] H. J. Dai, Y. J. Zhao, and C. Yu, "A multi-elements chessboard random coded metasurface structure for ultra-wideband radar cross section reduction," *IEEE Access*, vol. 8, article 2977630, 2020.

[15] X. Gao, X. Han, W. P. Cao, H. O. Li, H. F. Ma, and T. J. Cui, "Ultrawideband and high-efficiency linear polarization converter based on double V-shaped metasurface," *IEEE Transactions on Antennas and Propagation*, vol. 63, no. 8, pp. 3522–3530, 2015.

[16] Y. Q. Zhuang, G. M. Wang, and H. X. Xu, "Ultra-wideband RCS reduction using novel configured chessboard metasurface," *Chinese Physics B*, vol. 26, no. 5, pp. 054101–054123, 2017.

[17] M. Z. Zhao, X. Li, G. X. Dong, and Y. Liu, "Wideband radar cross-section reduction using plasma-based checkerboard metasurface," *Plasma Science and Technology*, vol. 24, no. 8, article 085501, 2022.